Sliding of viscoelastic polymers drops: insights from experiments and numerical simulations

Silvia Varagnolo,* Daniele Filippi, Giampaolo Mistura, and Matteo Pierno†
Dipartimento di Fisica e Astronomia "G. Galilei" - DFA and Sezione CNISM, Università di Padova, Via Marzolo 8, 35131 Padova (PD), Italy

Mauro Sbragaglia‡
Dipartimento di Fisica, Università di Roma "Tor Vergata" and INFN , Via della Ricerca Scientifica, 1 - 00133 Roma RM (Italy)

(Dated: October 10, 2016)

The motion of non-Newtonian (liquid) drops over planar surfaces results in a complicated balance between interfacial forces and non linear dissipation, which has been scarcely inspected. In this work we investigated viscoelastic drops, made of polymer solutions, sliding over homogeneous, inclined surfaces. We considered aqueous solutions of polyacrylamide (PAA), a flexible polymer, forming non-Newtonian fluids characterised mainly by normal stress difference effects. We systematically explored polymers concentrations from 250 to 10000 ppm, corresponding to dilute and semi-dilute regimes, and studied the elastic response of the drops above the critical Bond number, i.e. the critical dimensionless force needed to depin the droplet. The impact of non-Newtonian rheology on the sliding process was shown through the relation between the average dimensionless velocity and the applied volume forces. Results from experiments were complemented with lattice Boltzmann numerical simulations, combining a Navier-Stokes (NS) description for the solvent with a micro-mechanical viscoelastic FENE-P model. The numerical simulations were helpful to elucidate the relative importance of the free parameters in the FENE-P model, and to visualise the distribution of the polymer feedback stresses during the motion of the drops. Thanks to these insights, it was possible to correlate the distribution of the stresses to the droplet shape and the corresponding sliding velocity.

PACS numbers: 47.55.D-, 47.11.-j, 47.50.-d, 47.57.Qk, 68.08.Bc, 83.60.Rs, 83.80.Rs
Keywords: Dynamic wetting, Sliding, Drop motion, non-Newtonian, Elastic polymer

arXiv:1610.02064v1 [cond-mat.soft] 6 Oct 2016

I. INTRODUCTION

Controlling and manipulating drops on open surfaces is a crucial step for applications in many fields, including chemistry, biomedicine, ink-jet printing, food and pharmaceutical industry[1–5]. The vast majority of such applications involve non-Newtonian fluids, e.g. polymer solutions, biological samples[6, 7], blood[8, 9] or inks[10], characterised by a non-linear response to external stresses, consisting either in a shear-dependent viscosity (shear thinning, shear thickening or yield stress fluids) or in elastic effects related to the appearance of normal stresses. Despite the wide spread of complex fluids, the research about the behaviour of non-Newtonian drops is quite recent and limited mainly to spreading[11–15], dynamic wetting[16–21], and impacting[22–27] on surfaces. To the best of our knowledge, only a few works [28, 29] analyze the dynamics of non-Newtonian drops sliding down an inclined surface. Generally, such studies consider simple model fluids exhibiting only one marked non-Newtonian behaviour (often shear thinning or normal stress fluids) in order to disentangle the role played by different non-Newtonian effects in comparison with a Newtonian reference. Spreading measurements[11–15] report very weak deviations from the Newtonian case, both for solutions having a shear-dependent viscosity and for normal stress fluids, suggesting that non-Newtonian features are not relevant in this kind of phenomena. On the other hand, dynamic wetting[30] observed by moving a solid tube in a cylinder of liquid is characterised by strong non-Newtonian deviations for shear thinning solutions and weaker effects in case of normal stress fluids. Shear thinning induces a reduction of viscous bending near the contact line and a lower drag of the solid surface on the fluid in the wedge like region with respect to a Newtonian reference having the same zero-shear viscosity[31, 32]. Elasticity present in Boger fluids promotes an increase of curvature near the contact line, even if differences between Newtonian and non-Newtonian liquids are very weak[30]. However the strongest differences between Newtonian and non-Newtonian drops are observed in the impact dynamics, probably because of the higher shear rate involved in such a phenomenon[8, 22–27, 33, 34]. The post impact spreading of a shear thinning drop is faster than a Newtonian fluid having the same zero-shear viscosity and slower than a Newtonian fluid having the same infinite viscosity. The subsequent recoil is slower than a Newtonian fluid with the same infinite viscosity and is highly dependent both on viscosity and on surface wettability. Generally, spreading occurs

* present address: PDRA Department of Chemistry - University of Warwick, United Kingdom CV4 7AL
† matteo.pierno@unipd.it
‡ sbragaglia@roma2.infn.it

at higher speed as if the fluid features a lower viscosity, while recoil dynamics is slower, as for a more viscous fluid[8, 25, 26, 32–34]. Normal stress fluids show negligible deviations from the Newtonian reference in the spreading phase, whereas bouncing and rebounding are highly suppressed and the receding contact line is retarded[10, 23, 24, 35, 36]. Shear thickening fluids exhibit even more unusual behaviours, regarding both dynamics and the final state, in particular the maximum deformation does not depend on the velocity[22]. The first paper[29] focused on the sliding of non-Newtonian drops considered polystyrene/acetophenone solutions moving down homogeneous silicon-coated glass where sliding is often affected by the presence of pearling. In such a regime, drops are generally found to slide faster than the silicon oil chosen as Newtonian reference. However, the rheological properties of the investigated polymer solutions are not accurately detailed and the comparison involves set of data extracted from different papers published by different groups. Recently, a comprehensive experimental and numerical study [28] analyzed the sliding of Xanthan aqueous solutions featuring a very markedly shear thinning viscosity, but also non negligible elastic effects, at least for high enough concentrations. The main difference between Xanthan and Newtonian fluids is observed in the relation between the Capillary number (i.e. the non-dimensional velocity) on the Bond number (that is the dimensionless gravity force): the Newtonian linear scaling is substituted by a sublinear increase at low Xanthan concentrations and even a plateau for the most concentrated solutions. Lattice Boltzmann simulations ascribed such a deviation to the presence of normal stresses developed in the drop during sliding.

In this work we further investigate the role played by elastic effects on the sliding dynamics by observing drops of polyacrylamide solutions characterised mainly by normal stress difference effects due to the elasticity of such polymer chains. The experimental results were explained and complemented with lattice Boltzmann simulations based on a micro-mechanical model of Finitely Extensible Nonlinear Elastic dumbbells with Peterlin's approximation (FENE-P), typically exploited to model a normal stress fluid.

The paper is organised as follows: section II deals with the experimental and numerical techniques applied in this study, the corresponding results are described in sections III and IV, while conclusions are reported in section V.

II. MATERIAL AND METHODS

A. Experiments

We dispersed the polyacrylamide (PAA, $M_w \sim 10^6$ g mol^{-1}, Sigma Aldrich) either in water or in a mixture of glycerol and water at a glycerol concentration of 80% w/w. In both cases, solutions have concentrations ranging in the dilute or semi-dilute regime [11, 12, 37] as listed in Table I. PAA is a flexible polymer forming non-Newtonian solutions characterised mainly by normal stress difference effects.

TABLE I. Viscosity of the non-Newtonian PAA solutions, η_{os}, directly measured with glass capillary (Ostwald) viscometer.

Liquid	concentration (ppm w/w)	η_{os} (mPa s)
PAA/water	250	1.09±0.03
PAA/water	1500	2.09±0.06
PAA/water	2500	4.0±0.1
PAA/water	5000	9.1±0.3
PAA/water	10000	77±2
PAA/(glycerol/water 80%)	300	55±2

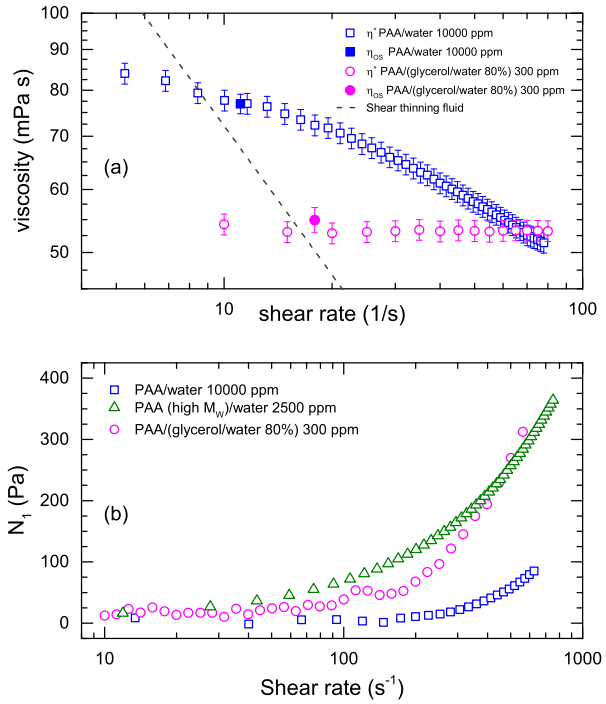

FIG. 1. Panel (a): Viscosity characterisation of the PAA solutions. η^* is the rheological measurement performed by a plate-plate rheometer at different shear rate. For comparison we also report η_{os}, the viscosity measured at fixed shear rate with a glass capillary viscometer (filled dots) and the viscosity of a power law fluid as a reference for a shear thinning fluid (dashed line). Panel (b): First Normal Stress difference of PAA solutions at different shear rate.

The viscosity of PAA solutions has been measured through two different methods, as shown in Figure 1 for the 1000 ppm PAA/water solution: i) The measurement performed with an Ostwald viscometer (η_{os}) provided an evaluation of the viscosity at a fixed shear rate (see Table I); ii) Using the rheometer the viscosity (η^*_{PAA}) was determined as a function of the shear rate, which is compatible with η_{os} for small shear rate ($\approx$ 1-10 s^{-1}) and then decreases. For concentrations up to 2500 ppm the viscos-

ity actually does not depend on the shear rate, in agreement with [12, 38]. At higher concentrations, η slightly varies with $\dot{\gamma}$ as shown in Figure 1a. This shear thinning effect is actually very weak, above all in comparison with shear thinning fluids, as for instance Xanthan solutions characterised by a viscosity depending on the shear rate through a power law [11, 12, 28]. In Figure 1a we also reported the viscosity of the PAA/(glycerol/water 80%) 300 ppm solution: in this case the shear thinning is completely suppressed and the viscosity is constant in the range of shear rate investigated [39]. Figure 1b analyses the elastic non-Newtonian behaviour of the same PAA solutions in terms of the first normal stress difference $N_1 = \tau_{11} - \tau_{22}$, being τ_{11} and τ_{22} the diagonal elements of the stress tensor. N_1 increases with the shear rate as a non-linear law in agreement with data reported in literature for similar PAA solutions [38]. Distilled water and glycerol/water solutions were chosen as the reference Newtonian fluids.

The substrate used in all experiments was a homogeneous, polycarbonate (PC) plate, whose wettability properties have been determined through the sessile droplet method[40]. The sample is characterised by a static contact angle θ close to 90° and dynamic contact angles similar for all solutions, as reported in the Supplementary Information (Table S1).

Sliding measurements of 30 μL drops have been performed by depositing the liquids on the already inclined sample and following the drop motion with a CMOS camera (MV-D1024E Camera Link), whose maximum frame rate is almost 120 fps [41]. Using a custom-made program we could identify the droplet contour, fitting it with a polynomial function, which is subsequently used to locate the front and rear contact points [40, 42]. The velocity of the steady-state motion was obtained by the temporal evolution of the front contact point [43, 44]. The sliding was observed at inclinations of the PC surface comprised between the critical sliding angle α_c (see below) and the highest angle for which volume control was still accurate. The appropriate dimensionless numbers required to compare the dynamics of drops of different fluids are suggested by the analysis of the sliding problem for Newtonian drops [45, 46], where the steady velocity U is the result of the balance between the external driving force and the viscous dissipation. Specifically, a Newtonian liquid droplet of volume V, viscosity η and density ρ, which slides down an inclined plane tilted by an angle α, is subject to the volume forces, the viscous drag and the interfacial forces. The volume force is proportional to the down-plane component of the droplet weigth, $\rho V g \sin\alpha$, while the viscous drag is proportional to $\sigma V^{1/3}\Delta_\theta$, where σ is the liquid-gas surface tension and Δ_θ depends on the perimeter-averaged projection of surface tension [28, 44]. Moreover, the non zero difference between the advancing and the receding contact angles for small velocities leads to contact angle hysteresis [47]. A critical inclination angle α_c exists above which the droplet depins and the balance of the gravity, viscous and capillary forces results in a linear scaling law [45, 46] between the *Capillary number* $\mathrm{Ca} = \eta \mathrm{U}/\sigma$ and the *Bond number* $\mathrm{Bo} = \mathrm{V}^{2/3}\rho \mathrm{g} \sin\alpha/\sigma$

$$\mathrm{Ca} \propto \mathrm{Bo} - \mathrm{Bo_c} \tag{1}$$

where $\mathrm{Bo_c} = \mathrm{V}^{2/3}\rho \mathrm{g} \sin\alpha_c/\sigma$ can be related to the wetting hysteresis via Δ_θ.

B. Numerical Simulations

To perform numerical simulations of polymeric fluids we used a Navier-Stokes (NS) description for the solvent coupled with constitutive equations for the stress tensor accounting for the (coarse grained) effects of polymer molecules. In particular, we adopted the FENE-P constitutive model, which hinges on a pre-averaging approximation applied to an ensemble of non interacting Finitely Extensible Nonlinear Elastic (FENE) dumbbells. This model is well-suited for dilute and semidilute polymeric solutions and has already been used in the literature (see [38, 48, 49] and references therein). We considered the diffuse-interface NS hydrodynamic equations of a binary mixture with 2 components [50, 51]. The hydrodynamical part of the model is obtained with a lattice Boltzmann model (LBM) [44], and allows the simulation of a droplet (d) with given dynamical viscosity η_d and density ρ_d sliding in an outer continuous (c) phase with dynamic viscosity η_c and density ρ_c [41, 44, 52]. We analysed the case of a two-dimensional droplet [53] with radius R, since this allows us to use larger numerical resolutions to well resolve hydrodynamics in the bulk phases. All the technical details for the LBM simulation of Newtonian drops are well described in our previous publication [44]. The non-Newtonian properties of the model have been validated in our recent works [54, 55] and the inclusion of the FENE-P rheology on the sliding has already been investigated in a previous publication from the authors [28], to preliminary elucidate the effects of normal stresses in comparison with thinning fluids. In this paper we take a step forward from the numerical point of view, in that we explore the effects of the FENE-P parameters (L^2 and τ_P, see below) on the sliding problem.

The relevant continuum equations which are solved inside the droplet are the NS equations coupled to the FENE-P equations:

$$\begin{aligned} \rho_d \left[\partial_t \boldsymbol{u}_d + (\boldsymbol{u}_d \cdot \boldsymbol{\nabla})\boldsymbol{u}_d\right] = &-\boldsymbol{\nabla} P_d + \\ &+ \boldsymbol{\nabla}\left(\eta_d(\boldsymbol{\nabla}\boldsymbol{u}_d + (\boldsymbol{\nabla}\boldsymbol{u}_d)^T)\right) + \\ &+ \frac{\eta_P}{\tau_P}\boldsymbol{\nabla}\cdot[f(r_P)\boldsymbol{C}] + \boldsymbol{g}\rho_d \sin\alpha \end{aligned} \tag{2}$$

$$\begin{aligned} \partial_t \boldsymbol{\mathcal{C}} + (\boldsymbol{u}_c \cdot \boldsymbol{\nabla})\boldsymbol{\mathcal{C}} = &\boldsymbol{\mathcal{C}}\cdot(\boldsymbol{\nabla}\boldsymbol{u}_c) + (\boldsymbol{\nabla}\boldsymbol{u}_c)^T\cdot\boldsymbol{\mathcal{C}} + \\ &- \frac{f(r_P)\boldsymbol{\mathcal{C}} - \boldsymbol{I}}{\tau_P} \end{aligned} \tag{3}$$

where P_d is the droplet bulk pressure while $\boldsymbol{u}_d$ is the hydrodynamic velocity and $(\boldsymbol{\nabla}\boldsymbol{u}_d)^T = \partial_j u_{d,i}$ is the trans-

pose of the tensor $\partial_i u_{d,j}$. In this model, the fluid total stress tensor is assumed to be the sum of a contribution from the solvent and another resulting from the presence of polymer molecules. The polymeric fluid shear viscosity is then the sum of polymeric (η_P) and solvent parts (η_d). The body force $\boldsymbol{g}\rho_d \sin\alpha$ is applied in the stream-flow (x) direction to mimic the effect of gravity down the inclined plane ($\boldsymbol{g} = (g, 0)$). The quantity $\boldsymbol{\mathcal{C}}$ is the polymer-conformation tensor, representing the average orientation and stretching of the polymers in the hydrodynamic flow. The characteristic polymer time τ_P regulates the relaxation of the conformation tensor towards its equilibrium value ($\boldsymbol{\mathcal{C}} = \boldsymbol{I}$). Moreover, FENE dumbbells can only be stretched by a finite amount, meaning that they possess a maximum extensional length squared L^2 and the FENE-P potential $f(r_P) \equiv (L^2 - 3)/(L^2 - r_P^2)$ that ensures finite extensibility ($r_p = Tr(\boldsymbol{\mathcal{C}})$).
In the continuous phase we only integrate the NS equations for the velocity $\boldsymbol{u}_c$

$$\rho_c \left[\partial_t \boldsymbol{u}_c + (\boldsymbol{u}_c \cdot \boldsymbol{\nabla})\boldsymbol{u}_c\right] = -\boldsymbol{\nabla} P_c + \\ + \boldsymbol{\nabla}\left(\eta_c(\boldsymbol{\nabla}\boldsymbol{u}_c + (\boldsymbol{\nabla}\boldsymbol{u}_c)^T)\right) \quad (4)$$

Regarding the non-ideal model used, we rely on the so-called "Shan-Chen" model [54, 56–58], ensuring phase segregation and the formation of diffuse interfaces with a positive surface tension. The model also allows for a tuning of the wetting properties at the fluid-solid interface (see [44] for details). In particular, we make use of a neutral wetting boundary condition and a Neumann boundary condition for the conformation tensor in contact with the flat substrate. A few comments are also in order, regarding the choice of the viscous ratio $\chi = \eta_c/(\eta_d + \eta_P)$. The use of very small viscosity ratios would be realistic, but is not easily achievable in the numerical simulations: numerical errors increase close to the interface [51] and this may affect the numerical results quite a lot. For the study at hand, we therefore decided to study the properties of viscoelastic drops ($\eta_P \neq 0$) and compare them with the corresponding Newtonian ($\eta_P = 0$) case by fixing the viscous ratio to unity, $\chi = 1$. For these cases the aforementioned deficiencies do not emerge.

III. EXPERIMENTAL RESULTS

In Figure 2a we report results from experiments, showing the dependence of the stationary droplet velocity U on the inclination angle α of the PC surface. The decrease of U as the polymer concentration increases is due to the higher viscosity of the more concentrated polymer solutions, which produces a smaller steady velocity [45–47, 59]. Hence, in order to compare the behaviour of the different liquids, it is more appropriate to plot data in terms of Ca versus Bo number. Given the weak dependence of η^* on U, to determine the Ca number we have assumed the constant value of viscosity η_{os} reported in Table I. The results are plotted in Figure 2b. PAA points corresponding to low inclinations follow the Newtonian linear trend, while at higher $\mathrm{Bo} - \mathrm{Bo_c}$ the Ca number stops increasing linearly and shows a sublinear behaviour, with a saturation in the Ca number at larger concentrations. In addition, PAA data collapse on the same curve, regardless of the polymer concentration. We point out that this analysis does not include shear thinning effects, which are present, although weak. Besides the time law, acquired snapshots can also give information about the droplet shape during the sliding, as shown in some examples reported in Figure 3. Both the side view (pictures a-c) and the bottom view (pictures a'-c') of the droplet can be useful to appreciate the shape deformation: for a fixed plane inclination PAA/water drops get elongated and develop a cornered rear tip, as observed also in [45] for Newtonian viscous oils. In addition, droplet stretching seems to become more pronounced as the PAA concentration increases. However, we would like to remark that droplet shape is highly sensitive to surface features such as wettability, homogeneity and cleanliness [60].

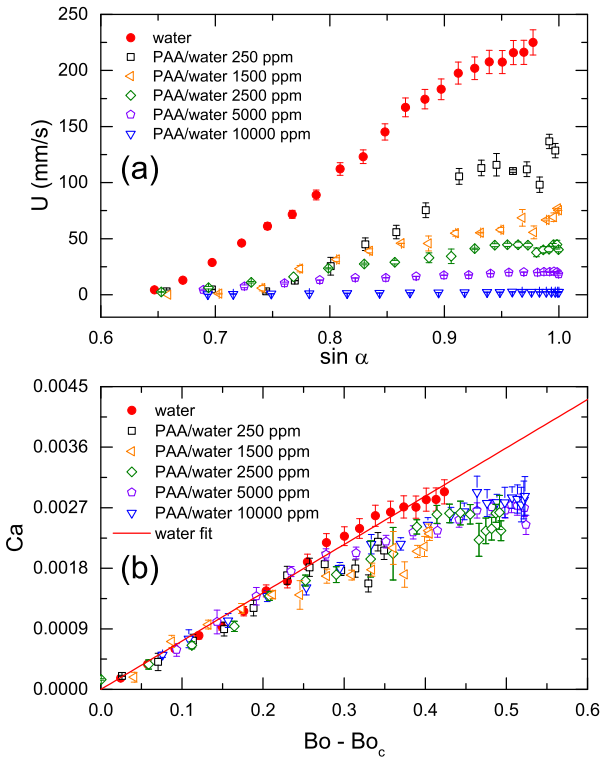

FIG. 2. Panel (a): Velocity of 30 μL drops sliding down the homogeneous plane (PC) inclined by different angles α for water and PAA/water solutions. Panel (b): dimensionless Ca *vs.* $\mathrm{Bo} - \mathrm{Bo_c}$ trend for water and PAA/water solutions. The viscosity used to calculate the Ca number is η_{os}. Line is a linear fit to the experimental data corresponding to the sliding of water drops, accordingly to Eq. 1.

For shear thinning liquids the viscosity inside the droplet is clearly dependent from the shear distribution inside the drop. Therefore, the computation of the Capillary number requires the viscosity to be determined for each sliding velocity U. A proficient, self-consisting

method to consider this effect in power law fluids has been proposed in [28]. Following a similar reasoning, we obtained an effective viscosity $\eta_{eff}(U)$ for PAA solutions, whose viscosity is only weakly dependent from the shear rate (see Figure 1). As a result, if for the calculation of the Ca number we take account also of the weak shear thinning effect, the resulting curves of Ca *vs.* $\mathrm{Bo} - \mathrm{Bo_c}$ will display a more pronounced plateau for the 5000 and 10000 ppm PAA solutions, while those at lower concentration would be barely affected (see Figure 4).

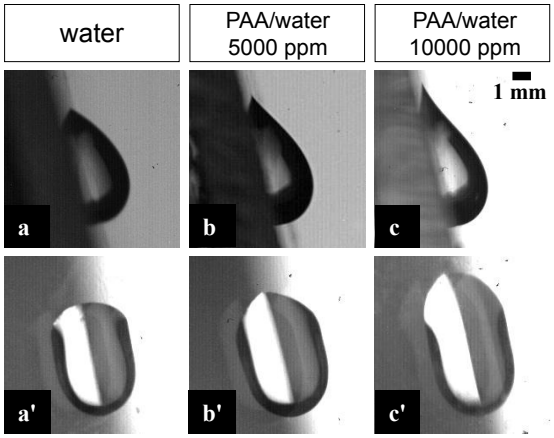

FIG. 3. Snapshots showing the side view (a-c) and bottom view (a'-c') of 30 μL drops sliding down a homogeneous PC surface inclined by the same angle (76°). While PAA/water drops get elongated, with an elongation more marked for the higher concentrations, water drops seem not to be affected by this deformation.

In order to shed light whether the non-linear dependence of the Ca on the Bo is due to shear thinning or normal stress difference, we repeated the same measurements using PAA/(glycerol/water 80%) solution, where the shear thinning is completely suppressed (see Figure 1a), and compare with a glycerol/water 85% solution, a Newtonian fluid featuring a similar viscosity. The corresponding dimensionless results are shown in Figure 5, where, again, the Newtonian sliding is characterised by a linear dependence between Ca and Bo, while the non-Newtonian solution presents only a very slight sublinear behaviour, with a Ca number systematically lower than the corresponding Newtonian one. Indeed, in this regime the effects of normal stress differences is masked by the onset of the capillary instability[61]: both Newtonian and non-Newtonian fluids are so viscous that pearling can likely occur and satellite microdrops form in the rear of the sliding drop, preventing to identify the drop's elongation induced by the polymer stretching, as expected for elastic, normal stress fluids (see insets in Figure 5).

Furthermore, we extended sliding measurements to viscoelastic aqueous solutions of PAA featuring a longer chain (PAA_{LC}, $M_w \sim 1.810^7$ g mol^{-1}, Polysciences, Inc.) and elastic effects stronger than the corresponding solutions of PAA with $M_w \sim 10^6$ g mol^{-1} (see Fig. 1).

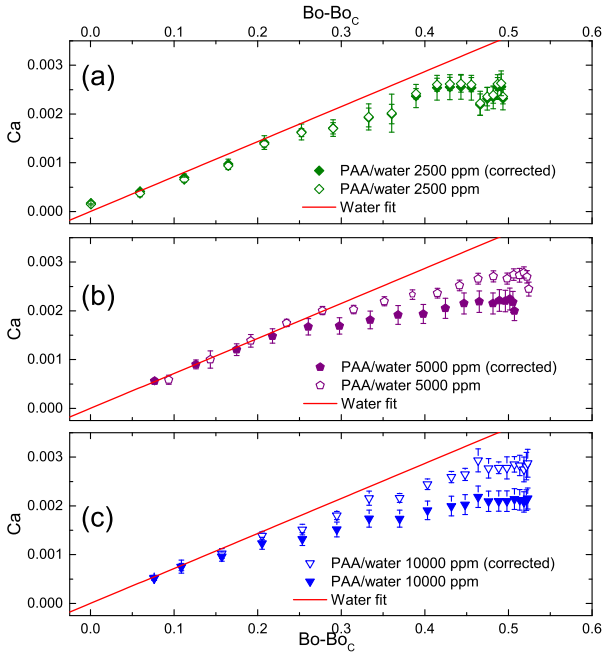

FIG. 4. Effects of the shear dependent viscosity on the computation of the Capillary number for PAA/water solutions at 2500 ppm (a), 5000 ppm (b), 10000 ppm (c).

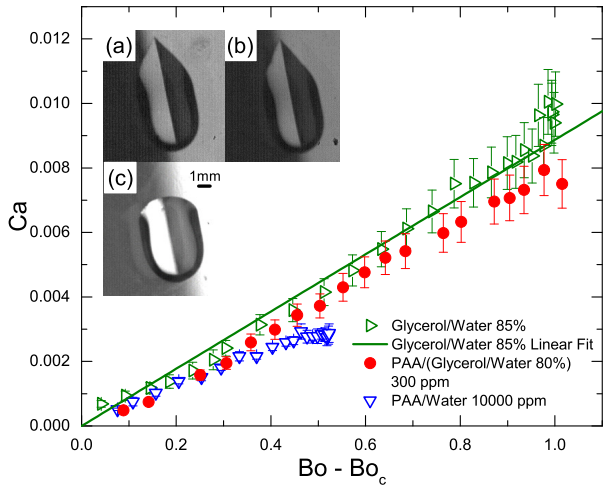

FIG. 5. Dimensionless Ca *vs.* $\mathrm{Bo} - \mathrm{Bo_c}$ curves for PAA/(glycerol/water) 300 ppm solution (the Boger fluid) in comparison to PAA/water solution 10000 ppm. The Newtonian reference is the mixture Glycerol/Water 85% w/w. The pictures show experimental images (taken from the bottom view) of a sliding drop: (a) is glycerol/water 85%, (b) is PAA/(gly/water 80%) 300 ppm solution and (c) is water, reported as a reference for the drops elongation.

In particular, we investigated PAA_{LC}/water 2500 ppm and we did not observe any slowing down of the sliding drop. To address this striking mismatch, it is useful to recall the study performed by Garoff and co-workers on dynamic wetting [62, 63]. Resuming, the polymers re-

action on the fluid takes some time to establish. If this time is large compared to the characteristic time of the fluid (i.e. the inverse shear), the polymers flowing in the drop wedge do not have enough time to develop a significant elastic stress. Thus, the strong shear of the contact line regions "favour" the feedback only of those polymers with characteristic times of the order of the local shear time [51]. This issue will be further unraveled by the numerical simulations (see Fig. 7 and Figures S1 and S2 of the Supplementary Information).

IV. NUMERICAL RESULTS

To complement the experimental data we have considered idealised models where viscoelastic effects can be tuned and visualised. This is here achieved with the help of numerical simulations. Even though the fluids we have considered in the numerical model differ from those of the real experiments, numerical simulations are quite useful to reveal the importance of viscoelastic stresses, including their distribution, which cannot be deduced from the experiment. We shall refrain from establishing a deeper quantitative connection between numerical simulations and experiments. In fact, we rather use numerical simulations to explore the effects of normal stresses in an idealised fluid where thinning effects are minimised. Specifically, for the problem of a FENE-P droplet, we can address systematically the importance of the various free parameters in the model (i.e. η_P, τ_P and L^2 see section II B) in promoting the emergence of sublinear (and plateau) behaviours in the Ca *vs.* $\mathrm{Bo}-\mathrm{Bo_c}$ curve, and also visualise the distribution of the polymer feedback stresses during the motion of the droplet, thus correlating the distribution of those stresses to the interface shape and the resulting macroscopic velocity. We started by showing that the shear rheology of the FENE-P model [64–66] is correctly reproduced for the parameters that we will use in our numerical investigation of sliding drops. The parameters η_P, τ_P and L^2 are free parameters in the FENE-P model and they can be tuned at will to obtain the desired rheology of the viscoelastic solution [65, 66]. The numerical model is benchmarked in panels of Figure 6: to this aim, we have recreated the bulk conditions of the droplet phase [1]. We have then measured the polymer shear viscosity η_S and the first normal stress difference N_1 resulting in a homogeneous steady shear with intensity $\dot\gamma$. Both N_1 and η_S are rescaled with the viscosity η_P, and they are plotted as a function of the dimensionless shear $\Lambda = \tau_P\dot\gamma$. Notice that the normal stress difference N_1 increases at large Λ and exhibits variable levels depending on L^2 [49, 65, 66].

Echoing the experimental results shown in Figure 2, we report in Figure 7 the Ca *vs.* Bo curve extracted from

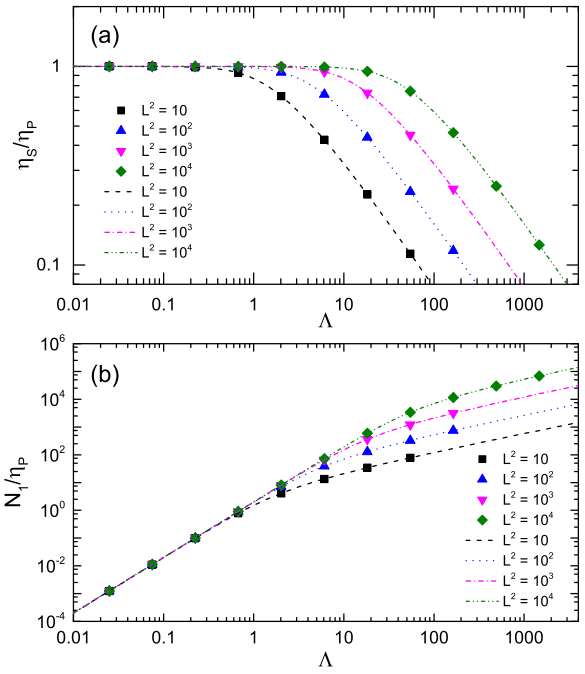

FIG. 6. Rheological characterisation for the numerical model. Symbols are results from numerical simulations (see text for details), dashed lines are the corresponding prediction from the FENE-P model [49, 65, 66] obtained for the same values of the extensibility parameter: $L^2 = 10$ (black, dashed line), $L^2 = 100$ (blue, dotted line), $L^2 = 1000$ (magenta, dash-dotted line), $L^2 = 10000$ (green, dash-dot-dotted line). Panel (a): polymer shear viscosity η_S developed in steady shear flow as a function of the dimensionless shear $\Lambda = \dot\gamma\tau_P$, $\dot\gamma$ being the shear rate and τ_P the polymer relaxation time (see section II B). Panel (b): first normal stress difference as a function of the dimensionless shear. Both η_S and N_1 are normalised with respect to the polymer viscosity η_P.

the steady state droplet velocity for various τ_P and L^2, at fixed $\beta = \eta_P/(\eta_d + \eta_P) = 0.2$. Figure 7a considers a fixed $L^2 = 5000$ [38] with various τ_P, the latter expressed in computational lattice Boltzmann units (lbu). A point of discussion emerges to judge how appropriate is the choice of the parameter τ_P in the FENE-P model. One expects viscoelastic effects to matter when the polymer relaxation time τ_P is of the order of the convective time scale, $\tau_{fluid} \approx \delta/U$, set by the characteristic velocity U and the characteristic length δ of the problem. For the sliding droplet, the characteristic velocity is taken from the sliding velocity, while we expect δ to be of the order of few interfaces widths for the diffuse interface methods [51]. For our numerical simulations we could sustain stable computations for a range of relaxation times τ_P such that τ_P/τ_{fluid} varies from values much below 1 to values close to 1 in the wedge close to the receding contact line. We remark that at larger τ_P and/or large Bo polymers are strongly stretched and develop large stress gradients, a fact that makes the numerical computations [51] not accessible in those conditions. In Figure 7a we illustrate

[1] Notice that this differs from the benchmark tests for single phase fluids performed in [54]

the effects introduced by the polymers for the aforementioned range of τ_P. At small Ca, the linear behaviour of the Ca *vs.* Bo curve is recovered for all the data, which nicely collapse on the same master curve. By increasing the driving force, however, a critical Ca exists around which the linear behaviour that is found for a Newtonian fluid is spoiled by viscoelasticity and a plateau emerges. Based on the data, we can indeed extract the characteristic velocity U_c at which the linear behaviour starts to be violated. We estimate that the linear behaviour is indeed lost when $\tau_P/\tau_{fluid} \approx 1$, i.e. when the ratio of the polymer relaxation time to the characteristic time of the fluid in the wedge close to the contact line is of the order one. This argument is reported in detail in Supplementary Information (Figure S1). Figure 7b reports the effect of an increase in L^2 for a fixed τ_P. It is readily verified that the deviations from linearity first emerge with a slight sublinear behaviour for the smallest L^2, while they produce a plateau for the largest L^2 ($L^2 \approx \mathcal{O}(10^3)$) [38, 49]. It is interesting to observe that the characteristic Ca at which the linear behaviour starts to be violated is only weakly dependent on the value of the finite extensibility parameter, while it is more vigorously dependent on the value of the polymer relaxation time, as can be appreciated in Figure 7a. The slight sublinear behaviour observed for $L^2 = 10^2$ Figure 7b is an indication that the driving force (gravity) is in balanced by two distinct effects, one linear in the velocity (viscous dissipation) and another quadratic in the velocity (normal stresses). However, although this idea can help in the understanding of the slight sublinear behaviour observed at small L^2 in Figure 7, it is not surely enough to get a deeper understanding for the plateau in the steady velocity as a function of the Bo number which is observed at the larger L^2. That behaviour somehow signals a "transition" in the dynamics of the sliding droplet, which can be corroborated with the analysis of the droplet shapes and polymer feedback stresses. This is done in Figure 8, where we report a simultaneous view of the stationary droplet shapes together with snapshots of the polymer feedback stresses for a fixed $L^2 = 5 \times 10^3$ and fixed Bo $= 0.024$, by varying the polymer relaxation time τ_P. We observe that viscoelastic effects are pronounced in the wedge flow close to the contact line while the bulk of the droplet behaves essentially as a Newtonian fluid. Normal stresses basically introduce an extra driving force for the flow near the contact line, and the effect is stronger upon increasing the shear rate, i.e. upon approaching the contact line region. This reduces the contact angle [12]. Since the sliding velocity varies with the contact angle, the lowering of the contact angle decreases the sliding velocity. For the largest τ_P (panel (c)), the emergence of viscoelastic stresses in the wedge region causes remarkable bending of the non-ideal interface near the moving contact line and the droplet gets visibly elongated. This argument is further supported by figure S2 in Supplementary Information.

We finally address the role of $\beta = \eta_P/(\eta_P + \eta_d)$ in Figure 7c. Variations with β amount to an increase in the contribution of the polymeric viscosity in the viscoelastic phase. Enhanced viscoelastic effects are thus expected for high β values [67, 68]. Indeed results shown in Figure 7c support this interpretation. The graph displays the Ca *vs.* Bo curve for various β ranging in the interval $[0.02, 0.40]$, at fixed $L^2 = 1 \times 10^4$ and $\tau_P = 10^3$ (lbu). Even at the smallest β the viscoelastic effects are not lost completely, while they saturate at larger β. Again, the characteristic Ca number at which the linear behaviour starts to be violated only weakly depends on β, supporting once more the idea that the deviation is substantially triggered by the polymer relaxation time τ_P, as already discussed for the data of Figure 7. These results echo the experimental findings reported in Figure 2, since larger η_P can be associated to larger polymer concentration [69, 70].

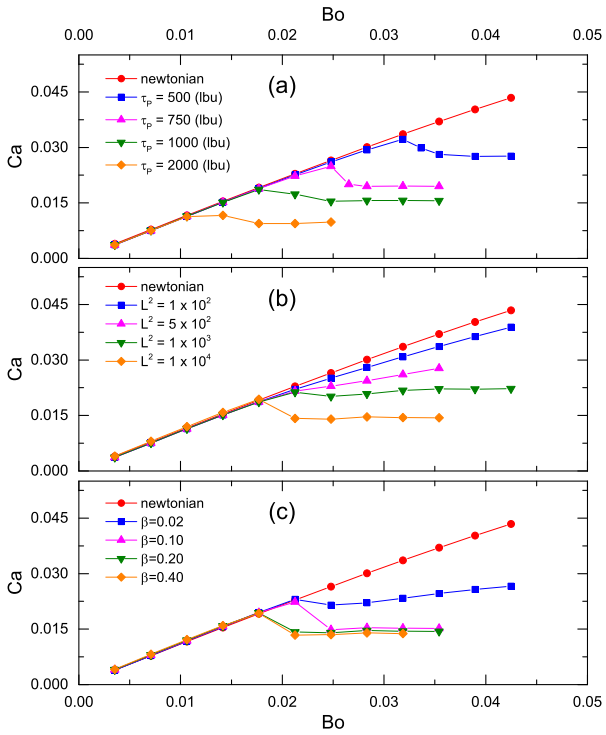

FIG. 7. Ca *vs.* Bo curves for different values of τ_P, L^2 and $\beta = \eta_P/(\eta_P + \eta_d)$ in the FEFE-P model (see section II B). Symbols are the results from the lattice Boltzmann numerical simulations, full lines are connections to the symbols as a guide for the eyes. Panel (a): Ca *vs.* Bo curve for various τ_P at fixed $L^2 = 5 \times 10^3$ and $\beta = 0.2$ (lbu). Panel (b): Ca as a function of the Bo for various L^2 at fixed $\tau_P = 10^3$ and $\beta = 0.2$ (lbu). Panel (c): Ca *vs.* Bo curve for different β at fixed $L^2 = 1 \times 10^4$ and $\tau_P = 10^3$ (lbu).

V. CONCLUSIONS

In this paper we have investigated non-Newtonian drops made of polymers in water solutions, sliding

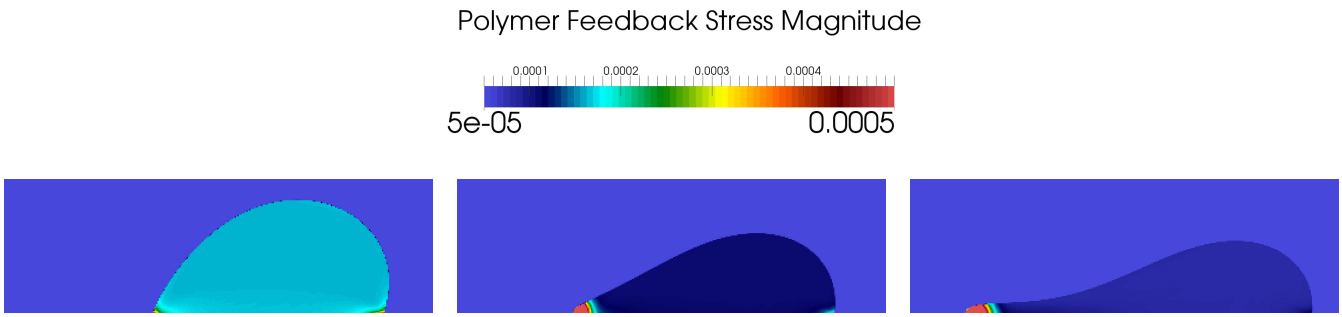

(a) Bo=0.024; $\tau_P = 500$ (lbu), $L^2 = 5 \times 10^3$

(b) Bo=0.024; $\tau_P = 1000$ (lbu), $L^2 = 5 \times 10^3$

(c) Bo=0.024; $\tau_P = 2000$ (lbu), $L^2 = 5 \times 10^3$

FIG. 8. Stationary droplet shapes and polymer feedback stresses inside the droplet obtained for $L^2 = 5 \times 10^3$ and Bo $= 0.024$ by varying the polymer relaxation time τ_P. Viscoelastic effects are pronounced in the wedge flow close to the contact line, while the bulk of the droplet behaves essentially as a Newtonian fluid. For large τ_P, the emergence of viscoelastic stresses in the wedge flow region causes an extra bending of the non-ideal interface near a moving contact line and the droplet gets elongated.

on a homogeneous inclined surface. In particular we considered solutions of polyacrylamide (PAA), a flexible polymer, exhibiting normal stress difference effects. Polymer solutions feature concentrations ranging in the dilute or semi-dilute regime. The sliding of non-Newtonian drops was compared with the one of water by systematically analyzing the relation between the Ca number and Bo number, which are the relevant dimensionless numbers used to characterize the Newtonian problem. The linear behaviour - which is peculiar of Newtonian solutions - was found to well adapt to the non-Newtonian solutions only up to a given Bo number, above which we found deviations, in that the linear behaviour was first replaced by a sublinear behaviour for small concentrations, and then by a more visible plateau. By properly rescaling the data, we argued that these effects can be mainly attributed to the presence of normal stress differences in the polymeric solutions. To complement the experimental data, we also performed numerical simulations of an "idealised" droplet with a dilute polymeric solution of non interacting Finitely Extensible Nonlinear Elastic dumbbells (FENE-P model). A parametric study performed in terms of the different model parameters (the polymer relaxation time τ_P, their maximum squared extensibility L^2 and their viscosity η_P) allowed to highlight the emergence of the observed experimental behaviours and visualise the distribution of the polymer feedback stresses during the motion of the droplet, thus correlating the distribution of those stresses to the interface shape and the resulting macroscopic velocity.

ACKNOWLEDGMENTS

The authors kindly acknowledge funding from the European Research Council under the European Community's Seventh Framework Programme (FP7/2007-2013)/ERC Grant Agreement No. 279004. We are particularly grateful to Michele Minchio, Chiara Guidolin and Rasa Platakyte for their help in the experimental work. In addition, we are indebted to Prof. Alessandro Martucci (University of Padova) and Prof. Giovanni Lucchetta (Department of Industrial Engineering, University of Padova) for the fruitful discussions and support about rheological characterisation. We acknowledge Anupam Gupta for support in the analysis of the numerical simulations. MS acknowledges useful discussions and fruitful exchange of ideas with Ciro Semprebon and Martin Brinkmann during their visit in September 2014.

[1] D. Quéré, *Annu. Rev. Mater. Res.*, 2008, **38**, 71–99.
[2] D. Bonn, J. Eggers, J. Indekeu, J. Meunier and E. Rolley, *Reviews of modern physics*, 2009, **81**, 739.
[3] K. Liu, X. Yao and L. Jiang, *Chem. Soc. Rev.*, 2010, **39**, 3240–3255.
[4] A. Bussonnière, M. Baudoin, P. Brunet and O. B. Matar, *Phys. Rev. E*, 2016, **93**, 053106.
[5] M. Sakai, T. Kato, N. Ishizuka, T. Isobe, A. Nakajima and A. Fujishima, *Journal of Sol-Gel Science and Technology*, 2016, **77**, 257–265.
[6] I. Barbulovic-Nad, S. H. Au and A. R. Wheeler, *Lab on a Chip*, 2010, **10**, 1536–1542.
[7] N. A. Mousa, M. J. Jebrail, H. Yang, M. Abdelgawad, P. Metalnikov, J. Chen, A. R. Wheeler and R. F. Casper, *Science Translational Medicine*, 2009, **1**, 1ra2–1ra2.
[8] N. Laan, K. G. de Bruin, D. Bartolo, C. Josserand and D. Bonn, *Physical Review Applied*, 2014, **2**, 044018.

[9] S. C. Shih, H. Yang, M. J. Jebrail, R. Fobel, N. McIntosh, O. Y. Al-Dirbashi, P. Chakraborty and A. R. Wheeler, *Analytical chemistry*, 2012, **84**, 3731–3738.

[10] Y. Son and C. Kim, *Journal of Non-Newtonian Fluid Mechanics*, 2009, **162**, 78–87.

[11] S. Rafai and D. Bonn, *Physica a-Statistical Mechanics and Its Applications*, 2005, **358**, 58–67.

[12] S. Rafai, D. Bonn and A. Boudaoud, *Journal of Fluid Mechanics*, 2004, **513**, 77–85.

[13] A. Carré and F. Eustache, *C. R. Acad. Sci. Paris*, 1997, **325**, 709–718.

[14] J. Han and C. Kim, *Journal of Non-Newtonian Fluid Mechanics*, 2013, **202**, 120–130.

[15] Q. Min, Y.-Y. Duan, X.-D. Wang, Z.-P. Liang, D.-J. Lee and A. Su, *Journal of colloid and interface science*, 2010, **348**, 250–254.

[16] X. Wang, D. Lee, X. Peng and J. Lai, *Langmuir*, 2007, **23**, 8042–8047.

[17] A. Boudaoud, *The European Physical Journal E*, 2007, **22**, 107–109.

[18] J. Han and C. Kim, *Rheol Acta*, 2014, **53**, 55–66.

[19] C. Liu, E. Bonaccurso, M. Sokuler, G. K. Auernhammer and H.-J. Butt, *Langmuir*, 2009, **26**, 2544–2549.

[20] Q. Min, Y.-Y. Duan, X.-D. Wang, Z.-P. Liang and D.-J. Lee, *International Journal of Thermophysics*, 2013, **34**, 2276–2285.

[21] A. Nakajima, *NPG Asia Materials*, 2011, **3**, 49–56.

[22] F. Boyer, E. Sandoval-Nava, J. H. Snoeijer, J. F. Dijksman and D. Lohse, *Physical Review Fluids*, 2016, **1**, 013901.

[23] D. Zang, W. Zhang, J. Song, Z. Chen, Y. Zhang, X. Geng and F. Chen, *Applied Physics Letters*, 2014, **105**, 231603.

[24] D. Zang, X. Wang, X. Geng, Y. Zhang and Y. Chen, *Soft Matter*, 2013, **9**, 394–400.

[25] V. Ravi, M. A. Jog and R. M. Manglik, *Interfacial Phenomena and Heat Transfer*, 2013, **1**, year.

[26] S. M. An and S. Y. Lee, *Experimental Thermal and Fluid Science*, 2012, **37**, 37–45.

[27] H. K. Huh, S. Jung, K. W. Seo and S. J. Lee, *Microfluidics and Nanofluidics*, 2015, **18**, 1221–1232.

[28] S. Varagnolo, G. Mistura, M. Pierno and M. Sbragaglia, *The European Physical Journal E*, 2015, **38**, 1–8.

[29] H. Morita, S. Plog, T. Kajiya and D. M., *Journal of the Physical Society of Japan*, 2009, **78**, 014804.

[30] Y. Wei, E. Rame, L. Walker and S. Garoff, *Journal of Physics: Condensed Matter*, 2009, **21**, 464126.

[31] Y. Wei, G. Seevaratnam, S. Garoff, E. Ramé and L. Walker, *Journal of colloid and interface science*, 2007, **313**, 274–280.

[32] G. Seevaratnam, Y. Suo, E. Ramé, L. Walker and S. Garoff, *Phys. Fluids*, 2007, **19**, 012103.

[33] G. German and V. Bertola, *Colloids and Surfaces A: Physicochemical and Engineering Aspects*, 2010, **366**, 18–26.

[34] J. H. Moon, D. Y. Kim and S. H. Lee, *Experimental Thermal and Fluid Science*, 2014, **57**, 94–101.

[35] M. Smith and V. Bertola, *Physical review letters*, 2010, **104**, 154502.

[36] M. Smith and J. Sharp, *Langmuir*, 2014, **30**, 5455–5459.

[37] P. T. Callaghan and A. M. Gil, *Macromolecules*, 2000, **33**, 4116–4124.

[38] P. Arratia, L.-A. Cramer, J. Gollub and D. J. Durian, *New J. Phys.*, 2009, **11**, 115006.

[39] L. Derzsi, M. Kasprzyk, J. P. Plog and P. Garstecki, *Physics of Fluids (1994-present)*, 2013, **25**, 092001.

[40] T. Toth, D. Ferraro, E. Chiarello, M. Pierno, G. Mistura, G. Bissacco and C. Semprebon, *Langmuir*, 2011, **27**, 4742–4748.

[41] S. Varagnolo, V. Schiocchet, D. Ferraro, M. Pierno, G. Mistura, M. Sbragaglia, A. Gupta and G. Amati, *Langmuir*, 2014, **30**, 2401–2409.

[42] D. Ferraro, C. Semprebon, T. Toth, E. Locatelli, M. Pierno, G. Mistura and M. Brinkmann, *Langmuir*, 2012, **28**, 13919–13923.

[43] S. Varagnolo, D. Ferraro, P. Fantinel, M. Pierno, G. Mistura, G. Amati, L. Biferale and M. Sbragaglia, *Physical Review Letters*, 2013, **111**, 066101.

[44] M. Sbragaglia, L. Biferale, G. Amati, S. Varagnolo, D. Ferraro, G. Mistura and M. Pierno, *Physical Review E*, 2014, **89**, 012406.

[45] T. Podgorski, J.-M. Flesselles and L. Limat, *Physical Review Letters*, 2001, **87**, 036102.

[46] H. Kim, H. Lee and B. Kang, *Journal of Colloid and Interface Science*, 2002, **247**, 372–380.

[47] C. Furmidge, *Journal of Colloid and Interface Science*, 1962, **17**, 309–324.

[48] C. Wagner, Y. Amarouchene, D. Bonn and J. Eggers, *Physical Review Letters*, 2005, **95**, 164504.

[49] A. Lindner, J. Vermant and D. Bonn, *Physica A*, 2003, **319**, 125–133.

[50] P. Yue, J. Feng, C. Liu and J. Shen, *J. Fluid Mech.*, 2004, **515**, 293–317.

[51] P. Yue and J. J. Feng, *Journal of Non-Newtonian Fluid Mechanics*, 2012, **189**, 8–13.

[52] H. Kusumaatmaja, J. Leopoldes, A. Dupuis and J. Yeomans, *Europhys. Lett.*, 2006, **73**, 740.

[53] N. Moradi, F. Varnik and I. Steinbach, *Europhys. Lett.*, 2011, **95**, 44003.

[54] A. Gupta, M. Sbragaglia and A. Scagliarini, *arXiv/1406.2686*, 2014.

[55] A. Gupta and M. Sbragaglia, *Physical Review E*, 2014, **90**, 023305.

[56] X. Shan and H. Chen, *Physical Review E*, 1993, **47**, 1815–1819.

[57] X. Shan and H. Chen, *Physical Review E*, 1994, **49**, 2941–2948.

[58] M. Sega, M. S. S. S. Kantorovich and A. O. Ivanovd, *Soft Matter*, 2013, **9**, 10092–10107.

[59] E. Rio, A. Daerr, B. Andreotti and L. Limat, *Physical Review Letters*, 2005, **94**, 024503.

[60] T. Sun, L. Feng, X. Gao and L. Jiang, *Accounts of Chemical Research*, 2005, **38**, 644–652.

[61] N. Le Grand, A. Daerr and L. Limat, *Journal of Fluid Mechanics*, 2005, **541**, 293–315.

[62] Y. Wei, G. Seevaratnam, S. Garoff, E. Ramé and L. Walker, *Journal of Colloid and Interface Science*, 2007, **313**, 274–280.

[63] Y. Wei, E. Ramé, L. Walker and S. Garoff, *J. Phys. Cond. Matt.*, 2009, **21**, 464126.

[64] R. Bird, P. Dotson and R. Armstrong, *Journal of Non-Newtonian Fluid Mechanics*, 1980, **7**, 213–235.

[65] R. B. Bird, R. C. Armstrong and O. Hassager, *Dynamics of polymeric liquids*, J. Wiley & Sons, 1987.

[66] M. Herrchen and H. Oettinger, *Journal of Non-Newtonian Fluid Mechanics*, 1997, **68**, 17–42.

[67] N. Aggarwal and K. Sarkar, *J. Fluid Mech.*, 2007, **584**, 1–21.

[68] N. Aggarwal and K. Sarkar, *J. Fluid Mech.*, 2008, **601**, 63–84.

[69] B. Purnode and M. Crochet, *Journal of Non-Newtonian Fluid Mechanics*, 1998, **77**, 1–20.

[70] B. Purnode and M. Crochet, *Journal of Non-Newtonian Fluid Mechanics*, 1996, **65**, 269–289.